CHEMISTRY OF MATERIALS

Article

pubs.acs.org/cm

Trimethylamine Borane: A New Single-Source Precursor for Monolayer h-BN Single Crystals and h-BCN Thin Films

Roland Yingjie Tay,[†,‡,¶] Hongling Li,[†,§,¶] Siu Hon Tsang,[‡] Minmin Zhu,[†,§] Manuela Loeblein,[†,§] Lin Jing,[∥] Fei Ni Leong,[†] and Edwin Hang Tong Teo*[,†,∥]

[†]School of Electrical and Electronic Engineering, Nanyang Technological University, 50 Nanyang Avenue, 639798, Singapore

[‡]Temasek Laboratories@NTU, 50 Nanyang Avenue, 639798, Singapore

[§]CNRS-International NTU Thales Research Alliance CINTRA UMI 3288, 50 Nanyang Drive, 637553, Singapore

[∥]School of Materials Science and Engineering, Nanyang Technological University, 50 Nanyang Avenue, 639798, Singapore

Supporting Information

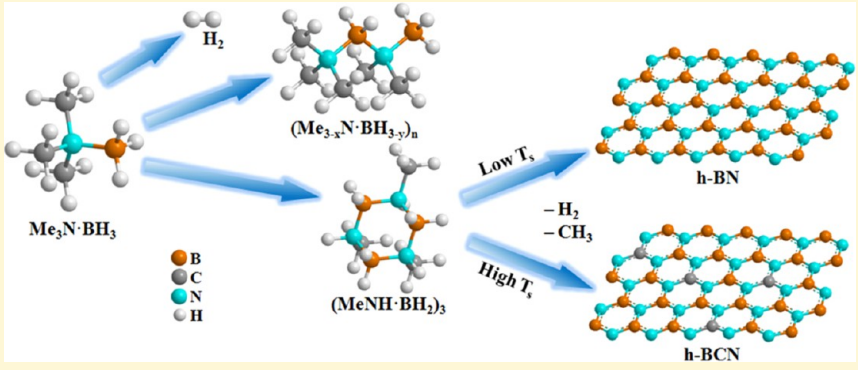

ABSTRACT: Due to their exceptional chemical and thermal stabilities as well as electrically insulating property, atomically thin hexagonal boron nitride (h-BN) films have been identified as a promising class of dielectric substrate and encapsulation material for high-performance two-dimensional (2D) heterostructure devices. Herein, we report a facile chemical vapor deposition synthesis of large-area atomically thin h-BN including monolayer single crystals and C-doped h-BN (h-BCN) films utilizing a relatively low-cost, commercially available trimethylamine borane (TMAB) as a single-source precursor. Importantly, pristine 2D h-BN films with a wide band gap of ∼6.1 eV can be achieved by limiting the sublimation temperature of TMAB at 40 °C, while C dopants are introduced to the h-BN films when the sublimation temperature is further increased. The h-BCN thin films displayed band gap narrowing effects as identified by an additional shoulder at 205 nm observed in their absorbance spectra. Presence of N−C bonds in the h-BCN structures with a doping concentration of ∼2 to 5% is confirmed by X-ray photoelectron spectroscopy. The inclusion of low C doping in the h-BN films is expected to result in constructive enhancement to its mechanical properties without significant alteration to its electrically insulating nature. This study provides new insights into the design and fabrication of large-area atomically thin h-BN/h-BCN films toward practical applications and suggests that the range of precursors can be potentially extended to other anime borane complexes as well.

INTRODUCTION

Hexagonal boron nitride (h-BN), which is also known as "white graphite" due to its similar honeycomb lattice structure,[1] exhibits many outstanding properties and is used in numerous practical applications.[2] Because it is unique as an insulator in the 2D family and coupled with its atomic smoothness and low density of surface dangling bonds, h-BN is widely used as a substrate or dielectric material for other 2D materials such as graphene and transition metal dichalcogenides (TMDs) for various high-performance 2D heterostructure devices.[3−6] In addition, due to its ability to withstand harsh conditions, h-BN is also used as an ultrathin encapsulation layer to prevent device degradation for materials which are more susceptive to oxidation such as black phosphorus (BP).[7−9]

Motivated by industrialization and the need for manufacturability, a variety of synthesis techniques to achieve atomically thin h-BN films over large distances have been explored such as chemical vapor deposition (CVD),[10−15] surface segregation method or solid source diffusion,[16−19] ion-beam sputtering deposition (IBSD),[20] pulsed-laser deposition (PLD),[21,22] reactive magnetron sputtering,[23] and molecular beam epitaxy (MBE).[24] Among them, CVD is the most commonly used due to its simplicity in design and operation. This matured synthesis technology, which has been extensively utilized in the

Received: January 11, 2016
Revised: March 10, 2016

DOI: 10.1021/acs.chemmater.6b00114
Chem. Mater. XXXX, XXX, XXX−XXX

绝缘性好，表面平滑，悬挂键少——衬底；
稳定性好——封装材料（BP）

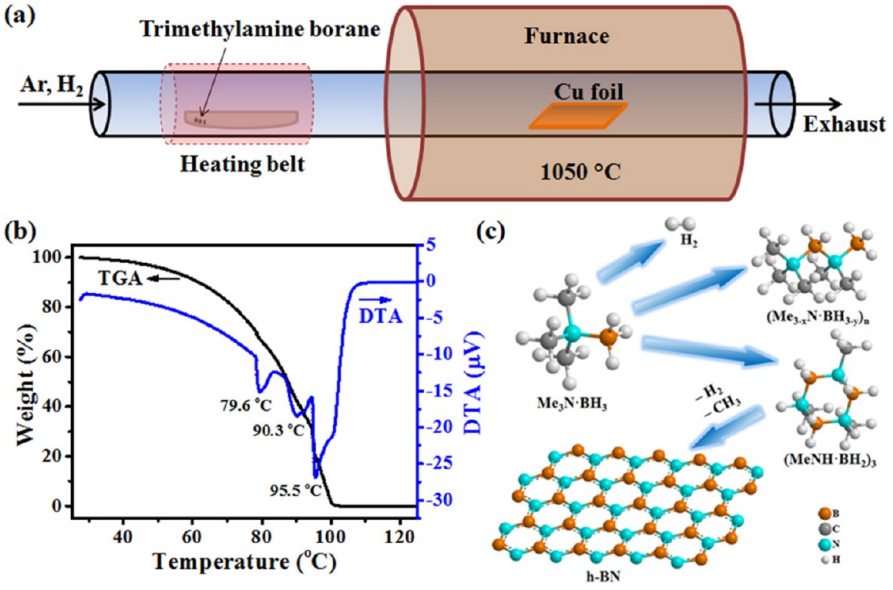

Figure 1. (a) Schematic layout of the CVD setup for h-BN/h-BCN film growth. (b) TGA (black trace) and DTA (blue trace) spectra of TMAB under an inert atmosphere. (c) Possible reaction pathways for the formation of h-BN by using TMAB as the single-source precursor.

semiconductor industry, would enable an easier transition toward mass production. Traditional B-containing gaseous precursors such as boron tribromide (BBr_3), boron trifluoride (BF_3), boron trichloride (BCl_3) and diborane (B_2H_6) together with ammonia (NH_3) as feedstock gases have been explored for BN film growth.[25−34] However, these B-containing compounds are highly toxic, which limits their further applications. Recently, ammonia borane (AB, NH_3−BH_3), which is much less toxic, has emerged as a successful single-source solid precursor for high-quality h-BN films due to its intrinsic 1:1 B/N stoichiometry and is used to obtain large-sized single-crystal domains which exceeds 100 μm in dimensions.[35−37] However, the most obvious drawback of using AB involves its very high cost, which is highly undesirable from a manufacturing perspective. Therefore, exploration and development of other alternatives with relatively low toxicity and cost as well as their corresponding processes for high-quality BN film growth remain an urgent need.

The synthesis of 2D C-doped BN (BCN) films, or vice versa, has also recently attracted immense research interest due to its capability for bandgap engineering, which is exceptionally useful for many electronics and optics applications.[38−40] However, most of the CVD synthesis methods rely on separate sources for BN and C, and the resultant film are often composed of small clusters of BN and C composites.[38] This thus restricts their overall tunability in terms of their optical and electrical properties. Herein, we report the synthesis of large-area atomically thin h-BN films including monolayer single crystals and few-layer C-doped BN (h-BCN) films by using trimethylamine borane (TMAB, $(CH_3)_3N{\cdot}BH_3$) as a single-source precursor. As TMAB contains all the required elements including B, N, and C in a single molecular, it has been previously used to fabricate mainly BCN films, while BN films can only be achieved with simultaneous inclusion of N-containing gases such as ammonia or N_2 plasma.[41−43] Although TMAB (with inherently 1:1 B/N stoichiometry, similar to AB) contains additional methyl groups (CH_3), we demonstrate that by refining the process, pristine h-BN monolayers and lightly doped h-BCN thin films with optical band gaps (OBGs) ranging from 6.13 to 5.92 eV can be controllably synthesized. The small decrease in OBG is associated with the slight increase in C doping concentration of ∼2 to 5% as determined by X-ray photoelectron spectroscopy (XPS). The obtained films are highly transparent with nearly 100% transmittance throughout the infrared and visible spectra as determined by ultraviolet−visible spectroscopy (UV−vis). Furthermore, the morphologies and structures of the as-prepared films are systematically characterized by scanning electron microscopy (SEM), atomic force microscopy (AFM), transmission electron microscopy (TEM), Raman, and Fourier transform infrared (FT-IR) spectroscopies.

EXPERIMENTAL SECTION

Synthesis of h-BN and h-BCN Films. Cu foils (Alfa Asear, product no. 13382, 25 μm thick) were used as growth substrates for the h-BN and h-BCN films. Prior to growth, the Cu foil was first dipped into dilute nitric acid for a few seconds and followed by rinsing with DI water to remove away the coatings on the Cu surface. The Cu foil was then loaded into a 1 in. quartz tube under a constant Ar/H_2 flow of 200:20 sccm. The furnace was ramped up to 1050 °C in 40 min and kept constant for another 30 min to anneal the Cu and to remove the surface oxide. After annealing, 10 mg of trimethylamine borane complex (Alfa Asear, product no. L14994, 97%), which was placed in a ceramic boat outside the heating zone, was heated at a specified temperature to commence the film growth. The growth time for monolayer h-BN single-crystal domains into a continuous film ranges from 5 to 20 min, while for h-BCN films, full coverage films are obtained after 5 min of growth due to the higher sublimation temperature used. After growth, the lid of the furnace was lifted for quick cooling.

Transfer Process. An electrochemical delamination process was used to transfer the films onto SiO_2/Si and quartz substrates. First, the as-grown h-BN or h-BCN film on Cu was spin coated with poly(methyl methacrylate) (PMMA) at 3000 rpm for 30 s. NaOH (1 M) was used as the electrolyte. A Pt foil was used as the anode, and the spin-coated sample was used as the cathode. A constant voltage of 5 V was applied until the

DOI: 10.1021/acs.chemmater.6b00114
Chem. Mater. XXXX, XXX, XXX−XXX

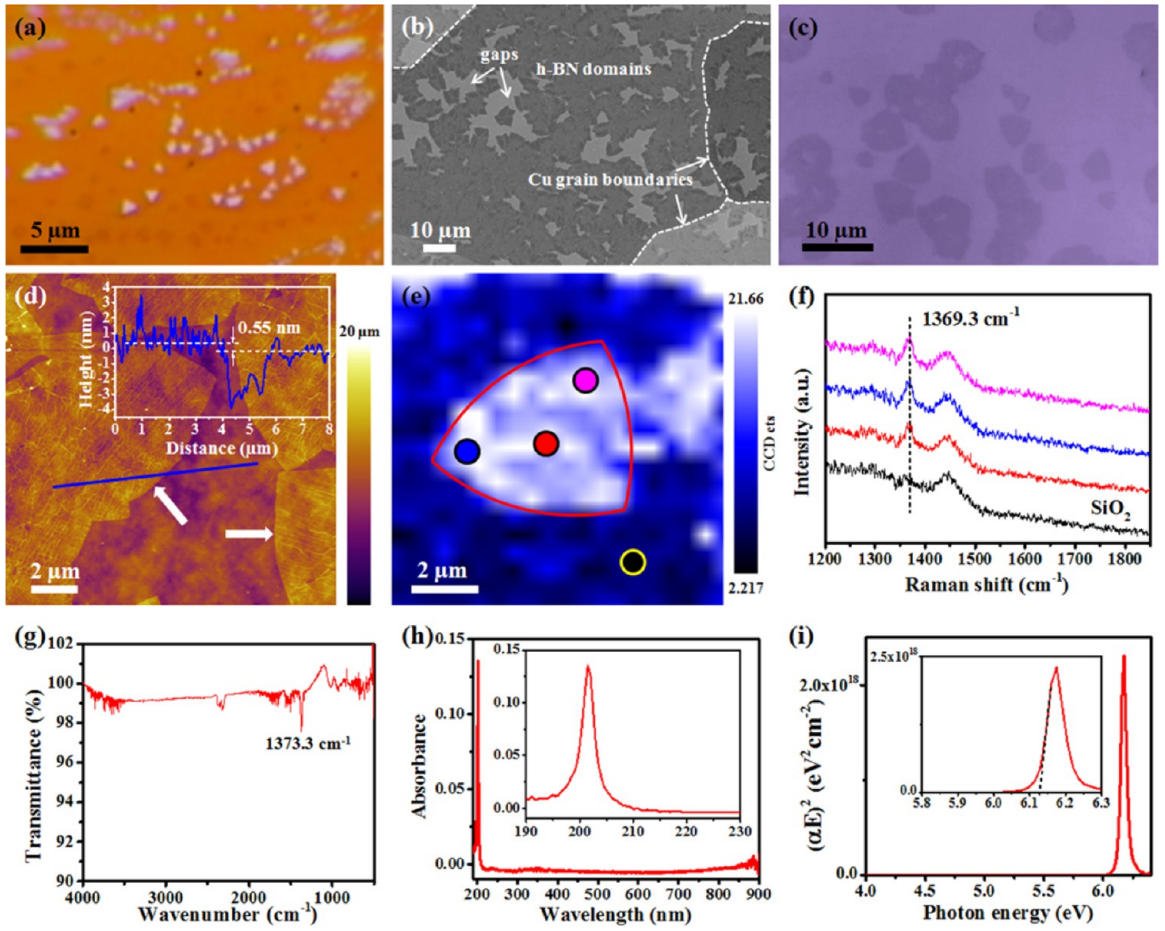

Figure 2. (a) Optical image of an air-oxidized h-BN/Cu. The brighter and the darker contrasts represent h-BN domains and oxidized Cu, respectively. (b) SEM image of the as-grown partially continuous h-BN film on a Cu substrate. (c) Optical image of the transferred h-BN domains on SiO_2/Si substrate. (d) AFM image of the transferred h-BN domains on SiO_2/Si substrate. The white arrows indicate the convexly curved edges and the inset shows the thickness of the film across the blue line. (e) Raman mapping of an individual h-BN domain. (f) Corresponding Raman spectra as indicated by the black, red, blue, and magenta spots in (e). (g) FT-IR spectrum of a monolayer h-BN. (h) Absorbance spectrum and its corresponding (i) Tauc's plot for OBG extraction of the monolayer h-BN.

PMMA coated sample is completely detached from the Cu. The sample was then rinsed in DI water for several times and transferred onto a desired substrate. The as-transferred sample was baked at 50 °C until it is completely dried. Finally, the PMMA is removed by submerging the sample in acetone for several hours.

Characterization. Thermogravimetric analysis (TGA, Shimadzu DTG-60H thermal analyzer) was used to determine the thermal decomposition profile of TMAB. The TGA measurement was carried out under a constant flow of nitrogen gas (100 mL/min) and heated from 25 to 125 °C at a heating rate of 2 °C/min. Scanning electron microscopy (SEM, LEO 1550 Gemini) images were taken directly on the as-grown h-BN and h-BCN films on Cu substrates. Atomic force microscopy (AFM, Cypher scanning probe microscope) was done using tapping mode to measure the thickness of the transferred h-BN and h-BCN films on SiO_2/Si substrates. Raman spectroscopy with laser excitation wavelength of 532 nm (Witec) was done at room temperature to determine the crystal structure of the transferred films on SiO_2/Si substrates. Fourier transform infrared spectroscopy (FT-IR, IRPrestige-21 spectrometer) was performed using the transferred h-BN film on a double-sided polished Si wafer within the wavenumber ranging from 4000 to 400 cm^{-1}. Transmission electron microscopy (TEM, Tecnai G2 F20 X-Twin) equipped with electron energy-loss spectroscopy (EELS) was operated with an acceleration voltage of 200 kV to determine the atomic structure and elemental composition of the h-BN film. X-ray photoelectron spectroscopy (XPS, PHI Quantera SXM Scanning X-ray Microprobe) was used to determine the elemental composition and bonding structures of the as-grown films on Cu. Ultraviolet−visible spectroscopy (UV−vis, Shimadzu UV-2450) was used to extract the optical band gaps (OBGs) of the transferred films on quartz substrates.

RESULTS AND DISCUSSION

Figure 1a shows the schematic layout of the atmospheric pressure (AP) CVD system used for the growth of monolayer h-BN single crystals as well as large-area (over centimeter-scale) atomically thin polycrystalline h-BN and h-BCN films formed by coalescence of multiple single-crystal domains. TMAB, one of the amine borane complexes, is used as a single-source precursor for all B, C, and N elements in the films, and Cu foils are used as catalytic substrates. As compared to AB, TMAB has a lower melting temperature due to the presence of the alkyl groups.[44,45] Therefore, the growth of the h-BN films can be realized by sublimating TMAB at a relatively lower sublimation temperature (T_s). Figure 1b shows the thermogravimetric

DOI: 10.1021/acs.chemmater.6b00114
Chem. Mater. XXXX, XXX, XXX−XXX

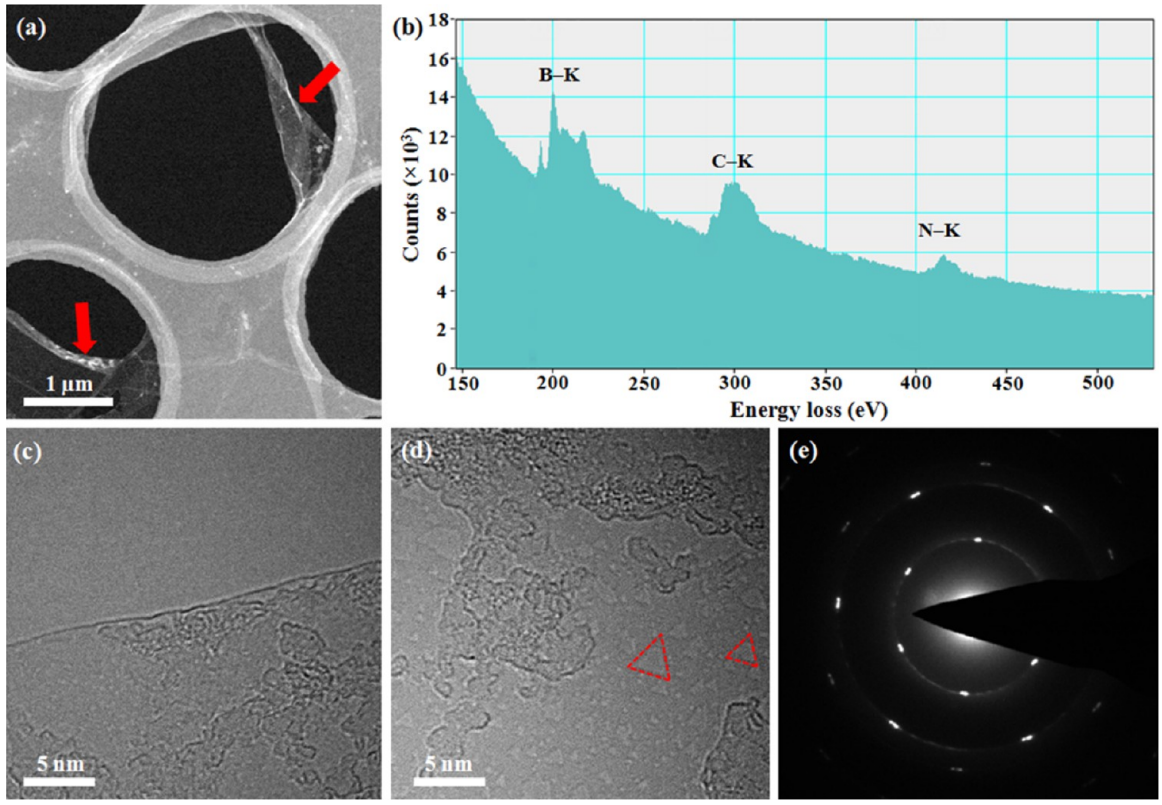

Figure 3. (a) Typical low-magnification TEM image of a transferred monolayer h-BN film on a TEM grid. (b) EELS spectrum of the h-BN film. High-magnification TEM images taken at the (c) edge and (d) interior of the transferred monolayer h-BN film. The red dashed outlines in (d) indicate triangular holes in the film. (e) Typical SAED pattern of the monolayer h-BN.

analysis (TGA) and its corresponding differential thermal analysis (DTA) spectra of TMAB under an inert atmosphere. A continuous weight loss occurs up to 100 °C with three endothermic peaks centered at 79.6, 90.3, and 95.5 °C, respectively, corresponding to the thermal decomposition/melting of TMAB with the loss of volatile gaseous including molecular hydrogen (H_2) and various dehydrogenated derivatives $(Me_{3-x}NBH_{3-y})_n$.[44,46,47] The possible dehydrogenation routes of TMAB and the pathway to form h-BN films are shown in Figure 1c. The dehydrogenation process begins across the B−N bonds, and the generated gaseous products of the TMAB decomposition can further polymerize and chemically transform inside the hot zone of the CVD tube. Cross-linking then starts occurring from the B sites which leads to the formation of trimeric aminoborane, $(MeNH{\cdot}BH_2)_3$.[47,48] Further intermolecular reactions of this compound through dehydrocoupling form cyclic chains with the framework of h-BN,[47,48] and 2D h-BN film will be produced by further cross-linking of these chains at above 1000 °C.[49] It should be noted that the cleavage of N−C bond is favored over B−N bond due to its relatively weaker chemical bond.[50] Meanwhile, the presence of H_2 gas will further aid the cleavage of N−C bonds,[51] which results in volatile CH_{3-x} during the formation of h-BN at high temperatures. This explains the negligible or small amount of C composition that exists in the as-prepared films. We also note that a catalytic substrate such as Cu is required for this formation process to enhance the dehydrogenation reaction as evident by the lack of h-BN film growth on SiO_2/Si substrates under the same growth conditions (Figure S1, Supporting Information).

Figure 2a shows an optical image of an air-oxidized h-BN/Cu foil to reveal the existence of h-BN domains during the initial stage of growth before they coalesce into a continuous film. As h-BN is highly resistant to oxidation,[9] the regions that are covered by the h-BN domains retained the same optical contrast as an nonoxidized Cu (brighter contrast) and the triangular shaped h-BN domains can be easily identified on the oxidized Cu. Figure 2b shows a typical SEM image of a partially continuous h-BN film formed by coalescing with neighboring domains. Figure 2c shows an optically enhanced image of the transferred h-BN domains on the SiO_2/Si substrate. Intriguingly, notable difference to the domain shape is observed on our h-BN as compared to most h-BN domains grown by using AB as precursor where they are composed of regular-shaped triangles with straight edges.[12] Instead, triangles with convexly curved edges or Reuleaux triangles are constantly observed for the h-BN domains grown using TMAB, which are further indicated by the white arrows in the AFM image of the transferred h-BN domains on SiO_2/Si substrate (Figure 2d). To explain the evolution of the curved edges of the h-BN domains, Wang et al. attributed such isotropic growth mechanism to the high concentration of adatoms along the circumference of the h-BN nuclei which can be controllably obtained by increasing the T_s of AB.[52] Since TMAB has a lower melting temperature than AB, the sublimation can occur at a faster rate when a smaller increase in T_s is applied. This is evident in the TGA profile of TMAB where the gradient of weight loss increases with increasing temperature (Figure 1b). In addition, as our growth is done using AP, this could further facilitate the supply of precursor to the growth substrate and hence, resulting in enhanced attachment kinetics. The inset of Figure 2d shows the

DOI: 10.1021/acs.chemmater.6b00114

通过控制AB加热温度，控制h-BN周围吸附原子浓度，从而控制BN形状

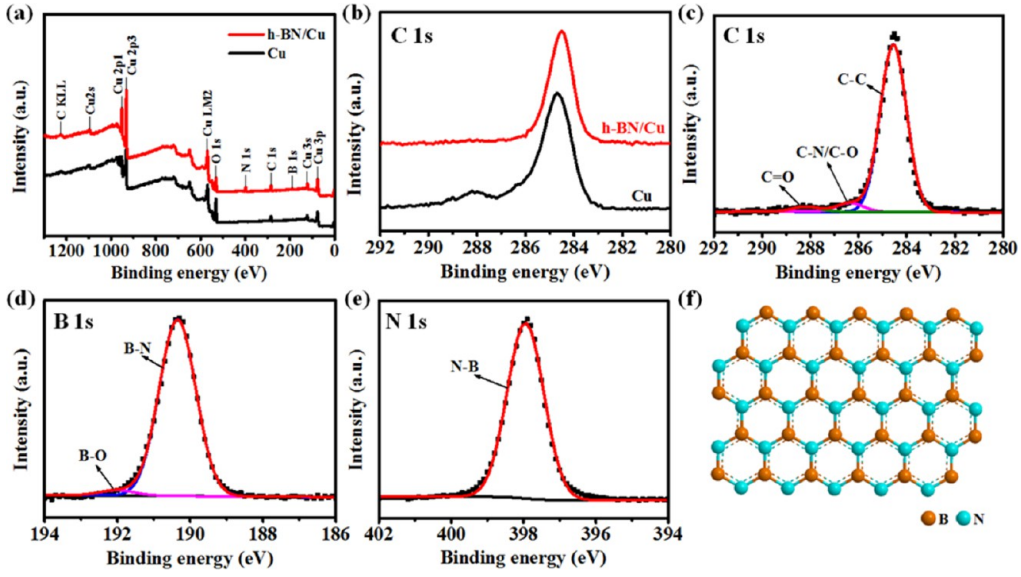

Figure 4. (a) XPS survey spectra and their corresponding (b) C 1s spectra of an as-grown h-BN/Cu (red trace) and an annealed bare Cu (black trace). (c–e) Deconvoluted high-resolution C 1s, B 1s, and N 1s XPS spectra of the h-BN/Cu, respectively. (f) Chemical bonding structure of the h-BN film.

typical thickness of the h-BN is ~0.55 nm, corresponding to a monolayer.

Figure 2e shows the Raman peak intensity map of an individual h-BN domain between 1360 and 1380 cm^{-1}. As the intensity of the E_{2g} peak is very weak for monolayer h-BN, a slight nonuniformity to the color distribution within the domain is observed, attributing to the noise contributions when the integration time is set at 10 s for each scanned pixel. Figure 2f shows the corresponding Raman spectra taken at three random locations in the h-BN domain using a longer integration time of 30 s and accumulated twice, in comparison with the SiO_2 surface. It is observed that the Raman spectra within the h-BN domain are consistent with a peak located at 1369.3 cm^{-1}, corresponding to the E_{2g} vibration mode of monolayer h-BN.[53] The other peak at ~1450 cm^{-1} is assigned to the third-order transverse optical (TO) phonon mode of Si which is also observed on the SiO_2 surface.[54] Figure 2g shows a typical FT-IR spectrum for the monolayer h-BN with a distinctive peak at 1373.3 cm^{-1} corresponding to in-plane B–N stretching mode.[55,56] No peak at ~780 cm^{-1} corresponding to out-of-plane B–N–B bending mode is observed as this peak is reported to be three times weaker for h-BN films.[56] Furthermore, due to the low dimensionality of the film, this peak became undetectable due to the lack of out-of-plane motion.[55] UV–vis spectroscopy is used to determine the OBG of the h-BN film and detect the doping effect in the system.[38,57,58] Figure 2h shows the absorbance spectrum of the monolayer h-BN film. It is observed that the h-BN film has a single sharp peak at 201.5 nm, which is a typical signature for a pristine atomically thin h-BN.[12,13] To extract the OBG of the film, the absorbance spectrum is converted into Tauc's plot (Figure 2i) using a derived formula for direct band gap semiconductor.[59] The extracted OBG is 6.13 eV (Figure S2, Supporting Information), comparable to the theoretical value of 6.0 eV.[60]

TEM technique is employed to further identify the atomic structure and monolayer nature of the as-prepared h-BN films. Figure 3a shows a typical low-magnification TEM image of the transferred monolayer h-BN film on a TEM grid. Several folded regions, as indicated by the red arrows, can be observed at some regions of the film due to the transfer process. Figure 3b shows the electron energy-loss spectroscopy (EELS) spectrum of the h-BN film. Two absorption peaks commencing at 188 and 401 eV are observed, corresponding to the K-shell ionization edges of B and N, respectively, which are characteristic peaks for sp^2 hydridized B–N bonds.[10,61] Another absorption peak commencing at 284 eV is assigned to C–C bonds due to contamination from the poly(methyl methacrylate) (PMMA) residues which might have not been totally removed after the transfer process. The extracted N/B ratio is 1.03, which is very close to the ideal value of 1 for h-BN. Figure 3c,d shows the high-magnification TEM images at the edge and interior of the transferred h-BN film, respectively. A single layer at the edge of the h-BN film is clearly identified in Figure 3c. In addition, many nanosized triangle holes (outlined in red dashed lines in Figure 3d), which are generated due to electron knock-on damage can be observed on the film,[62,63] further demonstrating the monolayer nature of the h-BN film. To evaluate the crystallinity in the film, selected area electron diffraction (SAED) is carried out on the transferred h-BN film (Figure 3e). The SAED reveals six distinctive spots arranged in a hexagonal pattern, corresponding to the hexagonal structure as expected for h-BN films.

为什么是三角形的呢？

The elemental composition and chemical structure of the as-prepared film are further investigated by using XPS. To determine the amount of C content in our film, we did a systematic comparison between the XPS spectra of the h-BN/Cu and an annealed Cu which underwent the same growth condition but without exposure to TMAB. Figure 4a shows the XPS survey spectra of the h-BN/Cu and bare annealed Cu samples. It is observed that both samples contain Cu, O, and C, whereas additional B and N elements only exist in the h-BN/Cu sample. In addition, the O 1s peak with a relatively lower intensity is observed for the h-BN/Cu sample, attributing to the h-BN film which acts as a protective layer against oxidation for the underlying Cu substrate.[9] C 1s peak is detected in both samples due to the presence of C impurities in the Cu foils (Figure 4b). The more prominent shoulder at 288.1 eV for the

对照

DOI: 10.1021/acs.chemmater.6b00114
Chem. Mater. XXXX, XXX, XXX–XXX

annealed Cu is due to C═O bond, which is originated from the higher amount surface Cu oxide. As shown in Figure 4c, the C 1s spectrum of h h-BN/Cu can be deconvoluted into three peaks located at 284.5, 286.4, and 288.2 eV, which are assigned to C−C, C−N/C−O, and C═O bonds, respectively.[64,65] However, these peaks are not representative of the film structure as they can also be extracted from the bare annealed Cu foil. Therefore, we focus our study on the B 1s and N 1s spectra to further identify the bonding structure in the film. The N/B ratio extracted on the basis of the integral intensities of each element peak is 1.11, which is consistent with the above-mentioned value as identified by EELS. Figure 4d,e shows high-resolution XPS spectra of B 1s and N 1s as well as their corresponding fitted peak profiles. The deconvoluted B 1s spectrum distinguishes two peaks located at 190.3 and 192.1 eV, respectively. The main component centered at 190.3 eV corresponds to B−N bonding and the smaller shoulder at higher binding energy is assigned to B−O bonding.[66] The presence of B−O bonding can be attributed to surface impurities[58] or the defective sites in the h-BN film.[67] The fitted N 1s peak in Figure 4e reveals only one component at 398.0 eV accounting for N−B bonding.[66] Therefore, based on all the above-mentioned characterization and analysis, we can reasonably conclude that the as-obtained domains/partial films correspond well to h-BN monolayers with negligible amount of C impurities (Figure 4f).

Taken into account when using Cu as the growth substrate for h-BN, the main parameters which will affect the nucleation density of h-BN domains are the surface smoothness of the substrate, CVD pressure and the flow rate of the precursor.[13,14] In our CVD growth process, Cu foil was used as the substrate and the precursor flow rate was controlled by using a low sublimation temperature (T_s) of 40 °C under atmospheric pressure. It is observed that sporadic monolayer h-BN domains can be achieved by squelching the growth early before a continuous film is formed. To verify the growth mechanism of the h-BN film, a time-dependent study is conducted to observe the evolution from sporadic domains into a continuous film (Figure 5a−e). After 5 min of growth, the domain size is typically ∼2 μm in length with many nucleation along the uneven Cu surface (Figure 5a). By prolonging the growth time to 8 and 10 min (Figure 5b,c), the average size of the domains increase to ∼5 μm with obvious increase in nucleation sites forming patches of discontinuous films by coalescing with neighboring domains. It should be noted that the "white" particles observed in the SEM images (Figure 5a−c) are BN nanoparticles which were formed at the sublimation region (front end of the quartz tube) through vapor phase pyrolysis of the precursor similar to previous reports (Figure S3, Supporting Information).[12,68] Single-crystal domain is hardly observed when the growth time is further increased to 15 min (Figure 5d) and a continuous film covering the entire surface of the Cu substrate over centimeter distances is obtained after 20 min of growth (Figure 5e). The growth is not self-limited and does not cease after a monolayer is formed. Presence of nanosized triangular shaped adlayer islands (outlined in red) can be observed within the existing monolayer (Figure 5f). These islands are composed of few- to multilayer h-BN as verified by Raman (Figure S4, Supporting Information).

As it is known that a smoother surface increases the Gibbs free energy barrier, the nucleation of the h-BN domains can be further suppressed by using electropolished Cu substrates.[13] Figure 6a,b shows the SEM images of the h-BN domains on a

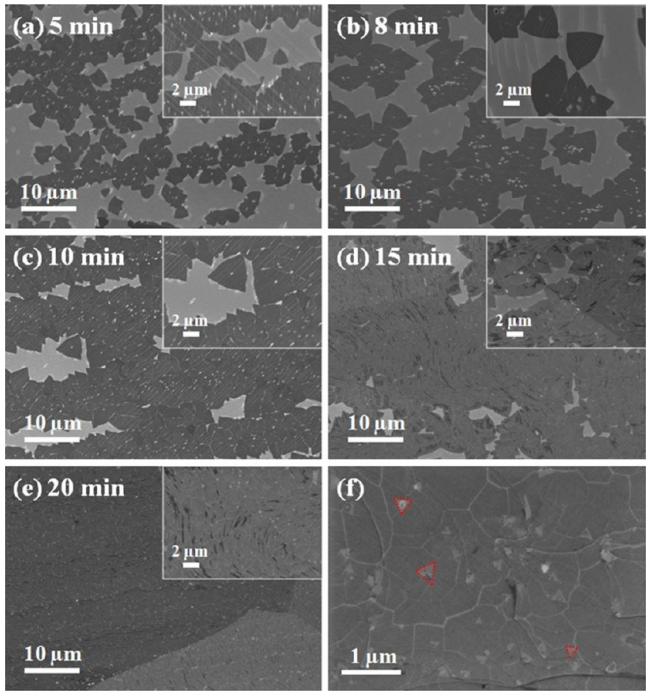

Figure 5. (a−e) SEM images of the as-grown h-BN on Cu after (a) 5, (b) 8, (c) 10, (d) 15, and (e) 20 min of exposure to TMAB at a T_s of 40 °C. The insets show their corresponding magnified SEM images. (f) High-magnification SEM image of (e) to reveal the adlayer triangular shaped islands.

polished and unpolished Cu, respectively, which were grown simultaneously for 8 min. An obvious decrease in nucleation density can be observed for the h-BN grown on polished Cu. The epitaxial relationship between the isolated single-crystal domains and the Cu lattice can be identified by mapping out their relative orientations (Figure S5, Supporting Information).[69,70] Various multifaceted complex structures consisting of multiple domains with grain boundaries or defect lines are observed due to the mirroring polarity of the domains (Figure 6c−e).[71,72] It has been reported that such structures are formed by either point-to-edge or edge-to-edge modes between two or more domains when they are nucleated close together.[52]

Few-layer continuous films using higher T_s were further grown and compared to the h-BN film that is grown using a T_s of 40 °C (Figure S6, Supporting Information). As shown in the DTA spectrum of TMAB (Figure 1b), the decomposition/melting of the precursor will occur at a faster rate when a higher temperature is used.[45] This results in the increase of volatile dehydrogenated products transported to the Cu substrate within a shorter time. We propose that the formation of BCN film is associated with the increased flow rate of the dehydrogenated derivatives and during the cross-linking process to form cyclic chains of h-BN, the methyl group may have played a more active role which forms chemical bonds within the h-BN structure, resulting in an increased density of N−C bonds. On the other hand, when a lower T_s of 40 °C is used, the growth of the film is relatively slower, and during the cross-linking process, cleavage of the N−C bonds is aided with the presence of H_2 gas.

The various films grown using T_s of 40, 50, 60, and 70 °C are denoted as BN40, BCN50, BCN60, and BCN70, respectively, hereafter. AFM scans show that the thicknesses of these BN and BCN films are similar and do not exceed 3 nm (Figure S7,

DOI: 10.1021/acs.chemmater.6b00114
Chem. Mater. XXXX, XXX, XXX−XXX

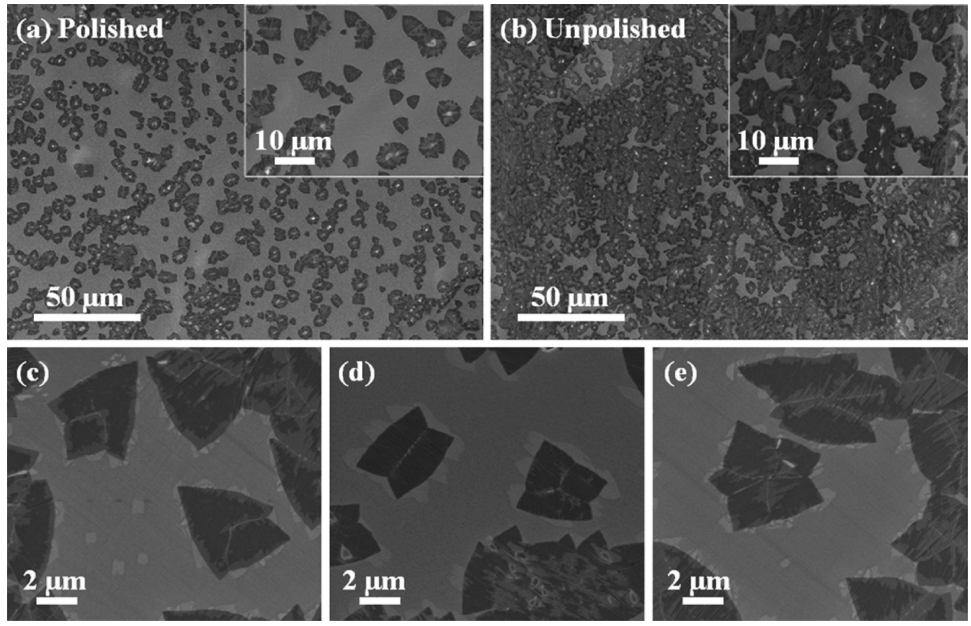

Figure 6. SEM images of as-grown h-BN domains on (a) polished and (b) unpolished Cu. The insets show their corresponding magnified SEM images. (c–e) Complex multifaceted structures of h-BN domains formed by coalescence between neighboring domains.

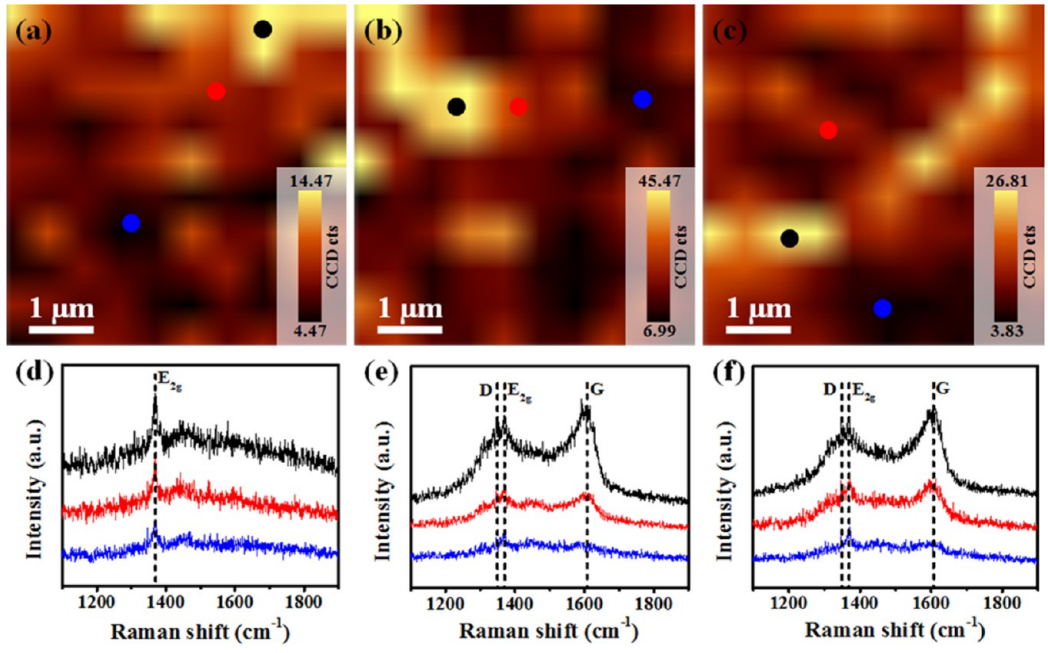

Figure 7. G peak intensity Raman mappings for (a) BCN50, (b) BCN60, and (c) BCN70 films transferred on SiO_2/Si substrates. (d–f) Corresponding Raman spectra as indicated by the black, red, and blue dots in (a–c), respectively.

Supporting Information). However, when the T_s is further increased to 80 °C and beyond, TMAB sublimates very quickly, and the resultant film surface becomes very rough with many particles and multilayer triangular shaped islands can be observed (Figure S8, Supporting Information). Therefore, to synthesize atomically thin films, the T_s of TMAB is limited to a maximum of 70 °C. Figure 7a–c shows the G peak intensity Raman mappings of the transferred BCN50, BCN60, and BCN70 films, respectively, on SiO_2/Si substrates ranging from 1580 to 1620 cm^{-1}. Figure 7d–f shows the corresponding Raman spectra at different locations indicated in black, red, and blue dots on the Raman maps in Figure 7a–c, respectively. As observed in Figure 7d, a single Raman peak at ~1370 cm^{-1} corresponding to h-BN is identified throughout the BCN50 film which is similar to that of BN40. Obvious disordered graphitic carbon peaks with broad D and G bands at ~1350 and ~1600 cm^{-1},[73] respectively, can be observed at many regions of the BCN60 and BCN70 films that are grown using higher T_s (Figure 7e,f), indicating that the films are likely to consist of carbonaceous content.

XPS is employed to provide further insights into the chemical structure and composition of the as-obtained BCN films. Figure 8a,b shows the deconvoluted B 1s and N 1s XPS spectra for BCN60, respectively. Two peaks located at 190.4

DOI: 10.1021/acs.chemmater.6b00114
Chem. Mater. XXXX, XXX, XXX–XXX

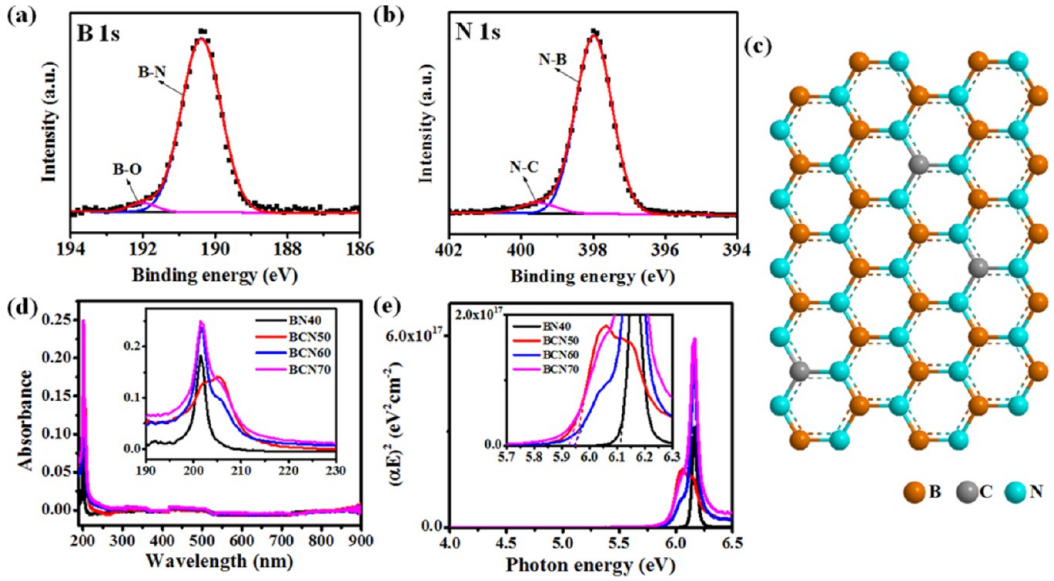

Figure 8. Deconvoluted high-resolution (a) B 1s and (b) N 1s XPS spectra for BCN60 film. (c) Chemical bonding structure of the h-BCN film. (d) UV−vis absorbance spectra and their corresponding (e) Tauc's plots for the various films grown using different T_s.

and 192.1 eV, similar to that in Figure 3d, can be fitted into the B 1s spectrum corresponding to B−N and B−O bonds, respectively (Figure 8a). For the N 1s spectrum, besides the main component composing of N−B bonding at 398.0 eV, a smaller shoulder at a higher binding energy of 399.6 eV arising from N−C bond is observed (Figure 8b).[38,58] The deduced chemical bonding structure of the film is presented in Figure 8c. The C atoms are "substituted" with the B atoms in the h-BN matrix as evident by the lack of B−C bond in the B 1s spectrum. It is logical that the film assumes this structure because N−C but not B−C bonds exist in the TMAB molecular. Based on the integrated characteristic deconvoluted peaks in the N 1s spectra of the h-BCN films, the estimated C doping concentration is ∼2 to 5%.

In order to study the optical properties and the band gap effects of the BN and BCN films, UV−vis spectroscopy is performed. It is observed that all the films are highly transparent with nearly 100% transmittance throughout the IR and visible spectra (Figure S9, Supporting Information). Figure 8d shows the absorbance spectra of the films grown at different T_s, and the inset shows the plot focusing at the deep UV region with wavelength ranging from 190 to 230 nm. It is observed that the BN40 film has a single sharp peak at 201.5 nm, corresponding to pristine atomically thin h-BN films.[12,13] For the other BCN films, an additional shoulder located at 205 nm is observed. This phenomenon is unlike the BN-doped graphene films, where the films contain composites of h-BN and graphene domains. In that case, two separate absorption peaks at 202 and 270 nm are observed, corresponding to h-BN and π plasmon peak of graphene, respectively.[38,40] For our BCN films, the presence of this shoulder indicates band gap narrowing effects due to substitutional doping. To extract the OBG of the films, the absorbance spectra are converted into Tauc's plots (Figure 8e). The extracted OBG for BN40 is 6.11 eV, whereas the OBGs of the BCN films that were grown at higher T_s fall among the ranges from 5.92 to 5.95 eV.

CONCLUSIONS

In summary, pristine monolayer h-BN single crystals as well as atomically thin h-BN and h-BCN films are successfully grown by CVD using a relatively low-cost, commercially available TMAB as a single-source precursor on Cu substrates. Importantly, by carefully varying the sublimation temperature (T_s) of the precursor, C doping concentration in the h-BN films can be controllably tuned. To synthesize pristine h-BN films, including monolayer single crystals, the T_s is limited to 40 °C, whereas further increasing the T_s will result in the formation of lightly doped h-BCN films due to the presence of uncleaved N−C bonds. The measured absorbance spectra of the h-BCN films exhibit an additional shoulder at 205 nm due to band gap narrowing effect caused by the C dopants. The C doping concentration in the h-BCN films is estimated at ∼2 to 5% as identified by XPS. By combining the existing results, the chemical structure of the h-BCN films grown using this method can be perceived as the B atoms are partially substituted by C atoms in an h-BN matrix. This work provides an alternative precursor source, which can be extended to other amine borane complexes, to fabricate h-BN/h-BCN films and enable tunability of its band gap by incorporation of C substitution. The h-BCN films could potentially offer a wider range of bandgap tunability for electronics and optics applications as well as provide constructive enhancement to the mechanical properties of the film.

ASSOCIATED CONTENT

Supporting Information

The Supporting Information is available free of charge on the ACS Publications website at DOI: 10.1021/acs.chemmater.6b00114.

Figures S1−S9, showing additional Raman, SEM, AFM, TEM, and UV−vis characterizations of the h-BN and h-BCN films prepared under different growth conditions (PDF)

DOI: 10.1021/acs.chemmater.6b00114
Chem. Mater. XXXX, XXX, XXX−XXX

AUTHOR INFORMATION

Corresponding Author

*E-mail: HTTEO@ntu.edu.sg. Tel: +65 67906371.

Author Contributions

¶These two authors contribute equally to this work (R.Y.T. and H.L.).

Notes

The authors declare no competing financial interest.

ACKNOWLEDGMENTS

The authors would like to acknowledge the funding support from NTU-A*STAR Silicon Technologies Centre of Excellence under the program grant No. 1123510003 and Singapore Ministry of Education Academic Research Fund Tier 2 No. MOE2013-T2-2-050.

REFERENCES

(1) Pease, R. S. Crystal Structure of Boron Nitride. *Nature* **1950**, *165*, 722−723.

(2) Lipp, A.; Schwetz, K. A.; Hunold, K. Hexagonal Boron Nitride: Fabrication, Properties and Applications. *J. Eur. Ceram. Soc.* **1989**, *5*, 3−9.

(3) Dean, C. R.; Young, A. F.; Meric, I.; Lee, C.; Wang, L.; Sorgenfrei, S.; Watanabe, K.; Taniguchi, T.; Kim, P.; Shepard, K. L.; Hone, J. Boron Nitride substrates for High-Quality Graphene Electronics. *Nat. Nanotechnol.* **2010**, *5*, 722−726.

(4) Britnell, L.; Gorbachev, R. V.; Jalil, R.; Belle, B. D.; Schedin, F.; Mishchenko, A.; Georgiou, T.; Katsnelson, M. I.; Eaves, L.; Morozov, S. V.; Peres, N. M. R.; Leist, J.; Geim, A. K.; Novoselov, K. S.; Ponomarenko, L. A. Field-Effect Tunneling Transistor Based on Vertical Graphene Heterostructures. *Science* **2012**, *335*, 947−950.

(5) Das, S.; Gulotty, R.; Sumant, A. V.; Roelofs, A. All Two-Dimensional, Flexible, Transparent, and Thinnest Thin Film Transistor. *Nano Lett.* **2014**, *14*, 2861−2866.

(6) Roy, T.; Tosun, M.; Kang, J. S.; Sachid, A. B.; Desai, S. B.; Hettick, M.; Hu, C. C.; Javey, A. Field-Effect Transistors Built from All Two-Dimensional Material Components. *ACS Nano* **2014**, *8*, 6259−6264.

(7) Avsar, A.; Vera-Marun, I. J.; Tan, J. Y.; Watanabe, K.; Taniguchi, T.; Castro Neto, A. H.; Özyilmaz, B. Air-Stable Transport in Graphene-Contacted, Fully Encapsulated Ultrathin Black Phosphorus-Based Field-Effect Transistors. *ACS Nano* **2015**, *9*, 4138−4145.

(8) Gillgren, N.; Wickramaratne, D.; Shi, Y.; Espiritu, T.; Yang, J.; Hu, J.; Wei, J.; Liu, X.; Mao, Z.; Watanabe, T.; Taniguchi, T.; Bockrath, M.; Barlas, Y.; Lake, R. L.; Ning Lau, C. Gate Tunable Quantum Oscillations in Air-Stable and High Mobility Few-Layer Phosphorene Heterostructures. *2D Mater.* **2015**, *2*, 011001.

(9) Liu, Z.; Gong, Y.; Zhou, W.; Ma, L.; Yu, J.; Idrobo, J. C.; Jung, J.; MacDonald, A. H.; Vajtai, R.; Lou, J.; Ajayan, P. M. Ultrathin High-Temperature Oxidation-Resistant Coatings of Hexagonal Boron Nitride. *Nat. Commun.* **2013**, *4*, 2541.

(10) Song, L.; Ci, L.; Lu, H.; Sorokin, P. B.; Jin, C.; Ni, J.; Kvashnin, A. G.; Kvashnin, D. G.; Lou, J.; Yakobson, B. I.; Ajayan, P. M. Large Scale Growth and Characterization of Atomic Hexagonal Boron Nitride Layers. *Nano Lett.* **2010**, *10*, 3209−3215.

(11) Shi, Y.; Hamsen, C.; Jia, X.; Kim, K. K.; Reina, A.; Hofmann, M.; Hsu, A. L.; Zhang, K.; Li, H.; Juang, Z.-Y.; Dresselhaus, M. S.; Li, L.-J.; Kong, J. Synthesis of few-layer hexagonal boron nitride thin film by chemical vapor deposition. *Nano Lett.* **2010**, *10*, 4134−4139.

(12) Kim, K. K.; Hsu, A.; Jia, X.; Kim, S. M.; Shi, Y.; Hofmann, M.; Nezich, D.; Rodriguez-Nieva, J. F.; Dresselhaus, M.; Palacios, T.; Kong, J. Synthesis of Monolayer Hexagonal Boron Nitride on Cu Foil using Chemical Vapor Deposition. *Nano Lett.* **2012**, *12*, 161−166.

(13) Tay, R. Y.; Griep, M. H.; Mallick, G.; Tsang, S. H.; Singh, R. S.; Tumlin, T.; Teo, E. H. T.; Karna, S. P. Growth of Large Single-Crystalline Two-Dimensional Boron Nitride Hexagons on Electropolished Copper. *Nano Lett.* **2014**, *14*, 839−846.

(14) Tay, R. Y.; Wang, X.; Tsang, S. H.; Loh, G. C.; Singh, R. S.; Li, H.; Mallick, G.; Teo, E. H. T. A Systematic Study of the Atmospheric Pressure Growth of Large-Area Hexagonal Crystalline Boron Nitride Film. *J. Mater. Chem. C* **2014**, *2*, 1650−1657.

(15) Tay, R. Y.; Tsang, S. H.; Loeblein, M.; Chow, W. L.; Loh, G. C.; Toh, J. W.; Ang, S. L.; Teo, E. H. T. Direct Growth of Nanocrystalline Hexagonal Boron Nitride Films on Dielectric Substrates. *Appl. Phys. Lett.* **2015**, *106*, 101901.

(16) Zhang, C.; Zhao, S.; Jin, C.; Koh, A. L.; Zhou, Y.; Xu, W.; Li, Q.; Xiong, Q.; Peng, H.; Liu, Z. Direct Growth of Large-Area Graphene and Boron Nitride Heterostructures by a Co-Segregation Method. *Nat. Commun.* **2015**, *6*, 6519.

(17) Zhang, C.; Fu, L.; Zhao, S.; Zhou, Y.; Peng, H.; Liu, Z. Controllable Co-Segregation Synthesis of Wafer-Scale Hexagonal Boron Nitride Thin Films. *Adv. Mater.* **2014**, *26*, 1776−1781.

(18) Suzuki, S.; Pallares, R. M.; Hibino, H. Growth of Atomically Thin Hexagonal Boron Nitride Films by Diffusion Through a Metal Film and Precipitation. *J. Phys. D: Appl. Phys.* **2012**, *45*, 385304.

(19) Xu, M.; Fujita, D.; Chen, H.; Hanagata, N. Formation of Monolayer and Few-Layer Hexagonal Boron Nitride Nanosheets via Surface Segregation. *Nanoscale* **2011**, *3*, 2854−2858.

(20) Wang, H.; Zhang, X.; Meng, J.; Yin, Z.; Liu, X.; Zhao, Y.; Zhang, L. Controlled Growth of Few-Layer Hexagonal Boron Nitride on Copper Foils Using Ion Beam Sputtering Deposition. *Small* **2015**, *11*, 1542−1547.

(21) Feng, P. X.; Sajjad, M. Few-Atomic-Layer Boron Nitride Sheets Syntheses and Applications for Semiconductor Diodes. *Mater. Lett.* **2012**, *89*, 206−208.

(22) Glavin, N. R.; Jespersen, M. L.; Check, M. H.; Hu, J.; Hilton, A. M.; Fisher, T. S.; Voevodin, A. A. Synthesis of Few-Layer, Large Area Hexagonal-Boron Nitride by Pulsed Laser Deposition. *Thin Solid Films* **2014**, *572*, 245−250.

(23) Sutter, P.; Lahiri, J.; Zahl, P.; Wang, B.; Sutter, E. Scalable Synthesis of Uniform Few-Layer Hexagonal Boron Nitride Dielectric Films. *Nano Lett.* **2013**, *13*, 276−281.

(24) Nakhaie, S.; Wofford, J. M.; Schumann, T.; Jahn, U.; Ramsteiner, M.; Hanke, M.; Lopes, J. M. J.; Riechert, H. Synthesis of Atomically Thin Hexagonal Boron Nitride Films on Nickel Foils by Molecular Beam Epitaxy. *Appl. Phys. Lett.* **2015**, *106*, 213108.

(25) Ismach, A.; Chou, H.; Ferrer, D. A.; Wu, Y.; McDonnell, S.; Floresca, H. C.; Covacevich, A.; Pope, C.; Piner, R.; Kim, M. J.; Wallace, R. M.; Colombo, L.; Ruoff, R. S. Toward the Controlled Synthesis of Hexagonal Boron Nitride Films. *ACS Nano* **2012**, *6*, 6378−6385.

(26) Younes, G.; Ferro, G.; Soueidan, M.; Brioude, A.; Souliere, V.; Cauwet, F. Deposition of Nanocrystalline Translucent h-BN Films by Chemical Vapor Deposition at High Temperature. *Thin Solid Films* **2012**, *520*, 2424−2428.

(27) Cheng, Y.; Yin, X.; Liu, Y.; Li, S.; Cheng, L.; Zhang, L. BN Coatings Prepared by Low Pressure Chemical Vapor Deposition using Boron Trichloride−Ammonia−Hydrogen−Argon Mixture Gases. *Surf. Coat. Technol.* **2010**, *204*, 2797−2802.

(28) Choi, B.; Park, D.; Kim, D. Preparation of Hexagonal Boron Nitride by Low Pressure Chemical Vapour Deposition in the BBr_3 + NH_3 + H_2 System. *J. Mater. Sci. Lett.* **1995**, *14*, 452−454.

(29) Coudurier, N.; Boichot, R.; Mercier, F.; Reboud, R.; Lay, S.; Blanquet, E.; Pons, M. Growth of Boron Nitride on (0001) AlN Templates by High Temperature-Hydride Vapor Phase Epitaxy (HT-HVPE). *Phys. Procedia* **2013**, *46*, 102−106.

(30) Pierson, H. O. Boron Nitride Composites By Chemical Vapor Deposition. *J. Compos. Mater.* **1975**, *9*, 228−240.

(31) Franz, D.; Hollenstein, M.; Hollenstein, C. Diborane Nitrogen/Ammonia Plasma Chemistry Investigated by Infrared Absorption Spectroscopy. *Thin Solid Films* **2000**, *379*, 37−44.

(32) Essafi, A.; Gomez-Aleixandre, C.; Albella, J. M. Study of Boron Nitride Deposition Process from Diborane and Ammonia Gas Mixtures. *Vacuum* **1994**, *45*, 1029−1030.

DOI: 10.1021/acs.chemmater.6b00114
Chem. Mater. XXXX, XXX, XXX−XXX

(33) Qin, L.; Yu, J.; Li, M.; Liu, F.; Bai, X. Catalyst-Free Growth of Mono-and Few-Atomic-Layer Boron Nitride Sheets by Chemical Vapor Deposition. *Nanotechnology* **2011**, *22*, 215602.
(34) Sano, M.; Aoki, M. Chemical Vapour Deposition of Thin Films of BN onto Fused Silica and Sapphire. *Thin Solid Films* **1981**, *83*, 247−251.
(35) Lu, G.; Wu, T.; Yuan, Q.; Wang, H.; Wang, H.; Ding, F.; Xie, X.; Jiang, M. Synthesis of Large Single-Crystal Hexagonal Boron Nitride Grains on Cu−Ni Alloy. *Nat. Commun.* **2015**, *6*, 6160.
(36) Yin, J.; Yu, J.; Li, X.; Li, J.; Zhou, J.; Zhang, Z.; Guo, W. Large Single-Crystal Hexagonal Boron Nitride Monolayer Domains with Controlled Morphology and Straight Merging Boundaries. *Small* **2015**, *11*, 4497−4502.
(37) Song, X.; Gao, J.; Nie, Y.; Gao, T.; Sun, J.; Ma, D.; Li, Q.; Chen, Y.; Jin, C.; Bachmatiuk, A.; Rümmeli, M. H.; Ding, F.; Zhang, Y.; Liu, Z. Chemical Vapor Deposition Growth of Large-Scale Hexagonal Boron Nitride with Controllable Orientation. *Nano Res.* **2015**, *8*, 3164−3176.
(38) Ci, L.; Song, L.; Jin, C.; Jariwala, D.; Wu, D.; Li, Y.; Srivastava, A.; Wang, Z. F.; Storr, K.; Balicas, L.; Liu, F.; Ajayan, P. M. Atomic Layers of Hybridized Boron Nitride and Graphene Domains. *Nat. Mater.* **2010**, *9*, 430−435.
(39) Song, L.; Liu, Z.; Reddy, A. L. M.; Narayanan, N. T.; Taha-Tijerina, J.; Peng, J.; Gao, G.; Lou, J.; Vajtai, R.; Ajayan, P. M. Binary and Ternary Atomic Layers Built from Carbon, Boron, and Nitrogen. *Adv. Mater.* **2012**, *24*, 4878−4895.
(40) Chang, C.-K.; Kataria, S.; Kuo, C.-C.; Ganguly, A.; Wang, B.-Y.; Hwang, J.-Y.; Huang, K.-J.; Yang, W.-H.; Wang, S.-B.; Chuang, C.-H.; Chen, M.; Huang, C.-I.; Pong, W.-F.; Song, K.-J.; Chang, S.-J.; Guo, J.-H.; Tai, Y.; Tsujimoto, M.; Isoda, S.; Chen, C.-W.; Chen, L.-C.; Chen, K.-H. Band Gap Engineering of Chemical Vapor Deposited Graphene by in Situ BN Doping. *ACS Nano* **2013**, *7*, 1333−1341.
(41) Baake, O.; Hoffmann, P. S.; Klein, A.; Pollakowski, B.; Beckhoff, B.; Ensinger, W.; Kosinova, M.; Fainer, N.; Sulyaeva, V. S.; Trunova, V. Chemical Character of BC_xN_y layers Grown by CVD with Trimethylamine Borane. *X-Ray Spectrom.* **2009**, *38*, 68−73.
(42) Kosinova, M. L.; Rumyantsev, Y. M.; Fainer, N. I.; Maximovski, E. A.; Kuznetsov, F. A. The Structure Study of Boron Carbonitride Films Obtained by use of Trimethylamine Borane Complex. *Nucl. Instrum. Methods Phys. Res., Sect. A* **2001**, *470*, 253−257.
(43) Rohr, C.; Boo, J. H.; Ho, W. The Growth of Hexagonal Boron Nitride Thin Films on Silicon using Single Source Precursor. *Thin Solid Films* **1998**, *322*, 9−13.
(44) Grant, D. J.; Matus, M. H.; Anderson, K. D.; Camaioni, D. M.; Neufeldt, S. R.; Lane, C. F.; Dixon, D. A. Thermochemistry for the Dehydrogenation of Methyl-Substituted Ammonia Borane Compounds. *J. Phys. Chem. A* **2009**, *113*, 6121−6132.
(45) Alton, E. R.; Brown, R. D.; Carter, J. C.; Taylor, R. C. Vapor Pressures of the Methylamine-Boranes and Ammonia-Triborane. *J. Am. Chem. Soc.* **1959**, *81*, 3550−3551.
(46) Bissot, T. C.; Parry, R. W. Preparation and Properties of Trimeric N-Methylaminoborane. *J. Am. Chem. Soc.* **1955**, *77*, 3481−3482.
(47) Bowden, M. E.; Brown, I. W. M.; Gainsford, G. J.; Wong, H. Structure and Thermal Decomposition of Methylamine Borane. *Inorg. Chim. Acta* **2008**, *361*, 2147−2153.
(48) Jaska, C. A.; Temple, K.; Lough, A. J.; Manners, I. Transition Metal-Catalyzed Formation of Boron−Nitrogen Bonds: Catalytic Dehydrocoupling of Amine-Borane Adducts to Form Aminoboranes and Borazines. *J. Am. Chem. Soc.* **2003**, *125* (31), 9424−9434.
(49) Fazen, P. J.; Remsen, E. E.; Beck, J. S.; Carroll, P. J.; McGhie, A. R.; Sneddon, L. G. Synthesis, Properties, and Ceramic Conversion Reactions of Polyborazylene. A High-Yield Polymeric Precursor to Boron Nitride. *Chem. Mater.* **1995**, *7*, 1942−1956.
(50) Dumont, H.; Bayle, B.; Bonnetot, B.; Bouix, J. Deposition and Characterization of BN/Si(0 0 1) using Tris(dimethylamino)borane. *Mater. Res. Bull.* **2002**, *37*, 1565−1572.
(51) Paine, R. T.; Narula, C. K. Synthetic Routes to Boron Nitride. *Chem. Rev.* **1990**, *90*, 73−91.
(52) Wang, L.; Wu, B.; Jiang, L.; Chen, J.; Li, Y.; Guo, W.; Hu, P.; Liu, Y. Growth and Etching of Monolayer Hexagonal Boron Nitride. *Adv. Mater.* **2015**, *27*, 4858−4864.
(53) Gorbachev, R. V.; Riaz, I.; Nair, R. R.; Jalil, R.; Britnell, L.; Belle, B. D.; Hill, E. W.; Novoselov, K. S.; Watanabe, K.; Taniguchi, T.; Geim, A. K.; Blake, P. Hunting for Monolayer Boron Nitride: Optical and Raman Signatures. *Small* **2011**, *7*, 465−648.
(54) Spizzirri, P. G.; Fang, J.-H.; Rubanov, S.; Gauja, E.; Prawer, S. Nano-Raman Spectrocopy of Silicon Surfaces; *Condensed Matter*, Cornell University Library; Article No. arXiv:1002.2692v1, **2010**.
(55) Geick, R.; Perry, C. H.; Rupprecht, G. Normal Modes in Hexagonal Boron Nitride. *Phys. Rev.* **1966**, *146*, 543−547.
(56) Jäger, S.; Bewilogua, K.; Klages, C. P. Infrared Spectroscopic Investigations on h-BN and Mixed h/c-BN Thin Films. *Thin Solid Films* **1994**, *245*, 50−54.
(57) Singh, R. S.; Tay, R. Y.; Chow, W. L.; Tsang, S. H.; Mallick, G.; Teo, E. H. T. Band Gap Effects of Hexagonal Boron Nitride using Oxygen Plasma. *Appl. Phys. Lett.* **2014**, *104*, 163101−4.
(58) Huang, C.; Chen, C.; Zhang, M.; Lin, L.; Ye, X.; Lin, S.; Antonietti, M.; Wang, X. Carbon-Doped BN Nanosheets for Metal-Free Photoredox Catalysis. *Nat. Commun.* **2015**, *6*, 7698.
(59) Yuzuriha, T. H.; Hess, D. W. Structural and Optical Properties of Plasma-Deposited Boron Nitride Films. *Thin Solid Films* **1986**, *140*, 199−207.
(60) Blase, X.; Rubio, A.; Louie, S. G.; Cohen, M. L. Quasiparticle Band Structure of Bulk Hexagonal Boron Nitride and Related Systems. *Phys. Rev. B: Condens. Matter Mater. Phys.* **1995**, *51*, 6868−6875.
(61) Chopra, N. G.; Luyken, R. J.; Cherrey, K.; Crespi, V. H.; Cohen, M. L.; Louie, S. G.; Zettl, A. Boron Nitride Nanotubes. *Science* **1995**, *269*, 966−967.
(62) Kotakoski, J.; Jin, C. H.; Lehtinen, O.; Suenaga, K.; Krasheninnikov, A. V. Electron Knock-on Damage in Hexagonal Boron Nitride Monolayers. *Phys. Rev. B: Condens. Matter Mater. Phys.* **2010**, *82*, 113404.
(63) Ryu, G. H.; Park, H. J.; Ryou, J.; Park, J.; Lee, J.; Kim, G.; Shin, H. S.; Bielawski, C. W.; Ruoff, R. S.; Hong, S.; Lee, Z. Atomic-Scale Dynamics of Triangular Hole Growth in Monolayer Hexagonal Boron Nitride under Electron Irradiation. *Nanoscale* **2015**, *7*, 10600−10605.
(64) Ronning, C.; Feldermann, H.; Merk, R.; Hofsäss, H.; Reinke, P.; Thiele, J. U. Carbon Nitride Deposited using Energetic Species: A Review on XPS Studies. *Phys. Rev. B: Condens. Matter Mater. Phys.* **1998**, *58*, 2207−2215.
(65) Estrade-Szwarckopf, H. XPS Photoemission in Carbonaceous Materials: A "Defect" Peak Beside the Graphitic Asymmetric Peak. *Carbon* **2004**, *42*, 1713−1721.
(66) Trehan, R.; Lifshitz, Y.; Rabalais, J. W. Auger and X-ray Electron Spectroscopy Studies of hBN, cBN, and N_2^+ Ion Irradiation of Boron and Boron Nitride. *J. Vac. Sci. Technol., A* **1990**, *8*, 4026−4032.
(67) Kidambi, P. R.; Blume, R.; Kling, J.; Wagner, J. B.; Baehtz, C.; Weatherup, R. S.; Schloegl, R.; Bayer, B. C.; Hofmann, S. In Situ Observations during Chemical Vapor Deposition of Hexagonal Boron Nitride on Polycrystalline Copper. *Chem. Mater.* **2014**, *26*, 6380−6392.
(68) Han, J.; Lee, J.-Y.; Kwon, H.; Yeo, J.-S. Synthesis of Wafer-Scale Hexagonal Boron Nitride Monolayers Free of Aminoborane Nanoparticles by Chemical Vapor Deposition. *Nanotechnology* **2014**, *25*, 145604.
(69) Liu, L.; Siegel, D. A.; Chen, W.; Liu, P.; Guo, J.; Duscher, G.; Zhao, C.; Wang, H.; Wang, W.; Bai, X.; McCarty, K. F.; Zhang, Z.; Gu, G. Unusual Role of Epilayer−Substrate Interactions in Determining Orientational Relations in van der Waals Epitaxy. *Proc. Natl. Acad. Sci. U. S. A.* **2014**, *111*, 16670−16675.
(70) Wood, E. G.; Marsden, J. A.; Mudd, J. J.; Walker, M.; Asensio, M.; Avila, J.; Chen, K.; Bell, R. G.; Wilson, R. N. van der Waals Epitaxy of Monolayer Hexagonal Boron Nitride on Copper Foil: Growth, Crystallography and Electronic Band Structure. *2D Mater.* **2015**, *2*, 025003.

DOI: 10.1021/acs.chemmater.6b00114
Chem. Mater. XXXX, XXX, XXX−XXX

(71) Auwarter, W.; Muntwiler, M.; Osterwalder, J.; Greber, T. Defect Lines and Two-Domain Structure of Hexagonal Boron Nitride Films on Ni(111). *Surf. Sci.* **2003**, *545*, L735−L740.
(72) Tay, R. Y.; Park, H. J.; Ryu, G. H.; Tan, D.; Tsang, S. H.; Li, H.; Liu, W.; Teo, E. H. T.; Lee, Z.; Lifshitz, Y.; Ruoff, R. S. Synthesis of Aligned Symmetrical Multifaceted Monolayer Hexagonal Boron Nitride Single Crystals on Resolidified Copper. *Nanoscale* **2016**, *8*, 2434−2444.
(73) Ferrari, A. C.; Meyer, J. C.; Scardaci, V.; Casiraghi, C.; Lazzeri, M.; Mauri, F.; Piscanec, S.; Jiang, D.; Novoselov, K. S.; Roth, S.; Geim, A. K. Raman Spectrum of Graphene and Graphene Layers. *Phys. Rev. Lett.* **2006**, *97*, 187401.

DOI: 10.1021/acs.chemmater.6b00114
Chem. Mater. XXXX, XXX, XXX−XXX